Nano Research

Open Access

Research Article

Submillimeter-scale atomic-thin metallic MoO_2 with noble metal-comparable SERS performance realized by thickness-dependent enhancement

Youzhe Bao[1], Jiamei Chen[1], Mengfan Ding[1], Jing Zhang[2], Xing Xin[1] ✉, Deming Cui[1], Wei Xin[1], Weizhen Liu[1] ✉, Peng Li[1], Jiangang Ma[1], Haiyang Xu[1] ✉, and Yichun Liu[1]

[1] *State Key Laboratory of Integrated Optoelectronics and Key Laboratory of UV Light-Emitting Materials and Technology of Ministry of Education, School of Physics, Northeast Normal University, Changchun 130024, China*
[2] *Institute for Interdisciplinary Quantum Information Technology, Jilin Engineering Normal University, Changchun 130052, China*

Cite this article: *Nano Research*, **2026**, *19*, 94908825. https://doi.org/10.26599/NR.2026.94908825

ABSTRACT: Metallic MoO_2 is promising to be one of noble-metal-comparable surface-enhanced Raman spectroscopy (SERS) substrate materials based on the strong electromagnetic mechanism (EM) enhancement. However, the SERS performance is still unable to meet the practical application requirements. Synthesizing large-scale two-dimensional (2D) metallic MoO_2 with controllable thickness, even at atomic level is an effective solution, but it has rarely been reported. The enhancement mechanism based on such kind of metallic metal oxide SERS substrates also lacks a more systematic study. Here, submillimeter-scale (~ 466 μm) atomic-thin (~ 4 nm) metallic MoO_2 was firstly synthesized by chemical vapor deposition (CVD). What's more, it shows high sensitivity as SERS substrates with a maximum enhancement factor up to 10^7 and a limit of detection down to 10^{-9} M, which is at a high level among most metal oxide-based SERS substrates and even comparable to the values of noble metal substrates with "hot spots". It was also firstly and systematically found that both the EM (surface plasmon resonance (SPR) effect) and chemical mechanism (CM) (charge transfer process) enhancements exist simultaneously in such MoO_2 substrate. The key lies in the thickness of MoO_2 that determines the dominant enhancement mechanism. MoO_2 flakes not only possess noble-metal-comparable SERS performance, but also show potential in image security and information encryption.

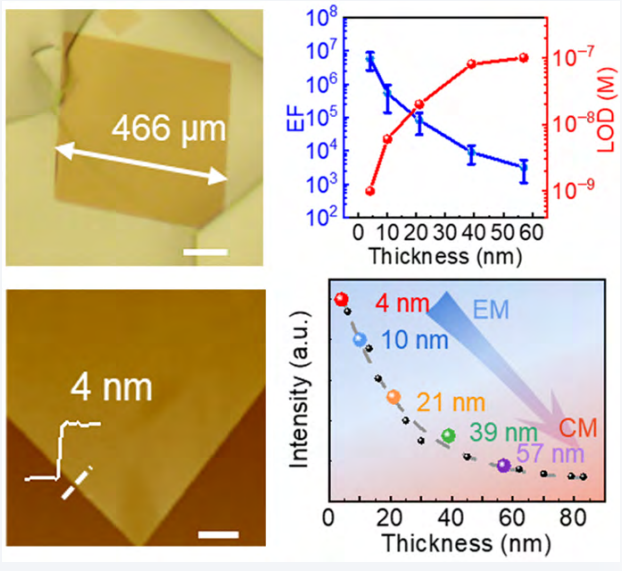

KEYWORDS: metal oxides, molybdenum dioxide, chemical vapor deposition, surface-enhanced Raman spectroscopy, two-dimensional (2D) materials

1 Introduction

The surface-enhanced Raman spectroscopy (SERS) is a powerful analysis technique for sensitive structural detection with trace concentration or even single-molecule levels, because it can significantly enhance Raman signals by several orders of magnitude than normal Raman [1–3]. SERS has already been widely used both in basic research fields and practical applications, such as biological sensing, catalysis chemistry, environmental monitoring, etc. [4–7]. There exist two accepted enhancement mechanisms in most reported studies, including electromagnetic mechanism (EM) and chemical mechanism (CM) [8]. EM as the primary one is induced by the local field magnification based on the surface plasmon resonance (SPR) of substrate materials [9]. Accordingly, noble metals with strong SPR effect such as Au and Ag, are used as

Received: March 11, 2026; **Revised:** May 7, 2026
Accepted: May 9, 2026

✉Address correspondence to Xing Xin, xinx902@nenu.edu.cn; Weizhen Liu, wzliu@nenu.edu.cn; Haiyang Xu, hyxu@nenu.edu.cn

traditional SERS substrates. When creating "hot spots" by fabricating rough surfaces or nanostructures of noble metals, an enhancement factor (EF) higher than 10^6 and a limit of detection (LOD) lower than 10^{-8} M can be obtained [10, 11]. However, such noble metal SERS substrates show poor biocompatibility and stability. The preparation of their nanostructures is also high-cost and the roughened surface morphology will inevitably produce non-uniform Raman signals [12].

Metal oxides are promising because of many excellent features, including low-cost, high chemical stability, and good biocompatibility. Recently, many kinds of metal oxide (e.g. TiO_2, ZnO, and Cu_2O) nanostructures have been reported as SERS substrates [13–15]. Unfortunately, most of them show relatively low EF (10–10^3) and poor LOD (10^{-3} M), falling far short of the requirements of the trace detection. These semiconducting metal oxides lack strong SPR effect and Raman enhancement is derived from the charge transfer between the analytes and SERS substrates, regarded as the CM. The weak CM-based enhancement can be improved with EF in the range of (10^4–10^6) and LOD in the range of (10^{-4}–10^{-9} M) by introducing high concentration of oxygen vacancy (such as TiO_{2-x} and $W_{18}O_{49}$) or preparing some special nanostructures (such as Cu_2O superstructure particle and TiO_2 microarray) [14, 16–18]. However, the thermal or chemical stability of these metal oxides are usually poor and their nanostructures will lead to non-uniform Raman signals. Some layered two-dimensional (2D) materials (e.g., graphene, MoS_2, and WTe_2) have also been applied on SERS [19–23]. Although they have shown certain advantages in terms of stability and uniformity, their SERS performance is still low due to the relatively weak CM-based enhancement. Therefore, the discovery of a more potential SERS substrate material with strong SPR effect as well as low cost, high stability and good uniformity is still challenging [24].

Different from most reported CM-based semiconducting metal oxides and 2D materials, metallic molybdenum dioxide (MoO_2) has a strong SPR effect because of the existence of numerous free electrons. Combined with its low-cost and high-stability feature, it is promising to be one of noble-metal-comparable SERS substrate materials [25]. It has been reported that the highest EF was up to 10^6 with detection limits of 10^{-6} to 10^{-8} M, when using some MoO_2-based nanostructures as SERS substrates [26]. However, the uniformity of SERS performance is still a problem due to their roughened surface morphologies. Preparing MoO_2 into large-scale 2D plates is likely an effective solution, but relevant works have rarely been reported at present. This is because MoO_2 as a kind of non-layered materials cannot be obtained by mechanically exfoliation from its bulk materials. Therefore, the large-scale preparation of these non-layered 2D materials with controllable thicknesses is inherently rather difficult [27]. The maximum grain size of currently reported 2D MoO_2 nanosheets by Wu et al. was only ~ 5 μm, with the minimum thickness of ~ 7 nm [28]. The corresponding maximum EF was also not high enough (~ 10^5) to match the practical requirements of applications, which may be caused by the insufficient thickness because the enhancement performance increases as the thickness decreases. Synthesizing large-scale 2D MoO_2 with controllable thickness, even at atomic level is promising for developing new SERS substrates with noble-metal-comparable SERS performance. On the other hand, although the thickness-dependent SERS performance of metallic MoO_2 has been reported, a comprehensive and systematic study on the thickness-related enhancement mechanism is still lacking [25, 27, 28].

Herein, we firstly synthesize large-scale 2D metallic MoO_2 flakes with controllable thicknesses by chemical vapor deposition (CVD). The maximum grain size is up to submillimeter level (~ 466 μm) and the minimum thickness is at atomic level of ~ 4 nm. What's more, these MoO_2 flakes show high sensitivity as SERS substrates with detected concentration down to 10^{-9} M and a maximum EF up to 10^7, which is at a high level among most metal oxide-based SERS substrates and even comparable to the values of noble metal substrates with "hot spots". Both the EM (SPR effect) and CM (charge transfer process) enhancements exist simultaneously in metallic 2D MoO_2 substrate, which is firstly and systematically reported. The key lies in its thickness that determines the dominant enhancement mechanism. The excellent SERS performance is realized by the thickness-dependent enhancement. In addition, MoO_2 flakes possess strong thermal and chemical stability after high-temperature (300 °C) heating in air and corrosion resistance in strong acid or alkali. They are universal for many commonly used chemicals, and exhibit high uniformity and good reproducibility of Raman signals. These characteristics not only provide their noble-metal-comparable SERS performance, but also make them potential in image security and information encryption.

2 Result and discussion

2.1 CVD growth of submillimeter-scale atomic-thin metallic MoO_2

Large-scale 2D MoO_2 flakes with controllable thicknesses were grown on Au foils by CVD, as shown in Fig. 1(a). Here, Au foils act as not only the growth substrates but also the catalysts that promote the growth process. MoO_3 and Se powders were used as precursor and reductant, respectively. 2D MoO_2 flakes were synthesized at high temperature (900 °C) in an Ar atmosphere. They are homogeneously distributed on the surface of Au and present a rhombic morphology with acute angle of ~ 81° (Fig. 1(b)). Details of preparation process were described in Experimental section and Fig. S1 in the Electronic Supplementary Material (ESM)). Au foils were reusable and barely affect the growth results as shown in Fig. S2 in the ESM. Interestingly, we found that the grain sizes and thicknesses of these flakes change with the amount of Se used gradually increasing from 30 to 110 mg. The grain size shows initially increases and then decreases, while the thickness presents the opposite tendency. Surprisingly, large-scale atomic-thin 2D MoO_2 with the maximum grain size of ~ 466 μm and the minimum thickness of ~ 4 nm can be obtained with a moderate usage of Se powder (70 mg), as shown in Figs. 1(c) and 1(d). To further confirm the above results, we statistically analyzed the morphological changes including both grain sizes and thicknesses under different Se dosages. The data in Fig. 1(e) was collected by measuring 20 samples randomly selected in each figure in Fig. S3 in the ESM, which shows the same tendency. We have also made a comparison with the reported results about 2D metal oxides in Fig. 1(f). Obviously, our results show advantages both in terms of grain size and thickness control, which is very difficult and rarely reported for 2D non-layered metal oxides.

2.2 Structural characterization of 2D MoO_2

Raman spectroscopy and X-ray photoelectron spectroscopy (XPS) were preliminary used to characterize the structure information of MoO_2 flakes. As shown in Fig. 2(a), there are nine typical Raman peaks located at 124, 202, 228, 343, 362, 457, 495, 567 and 740 cm^{-1},

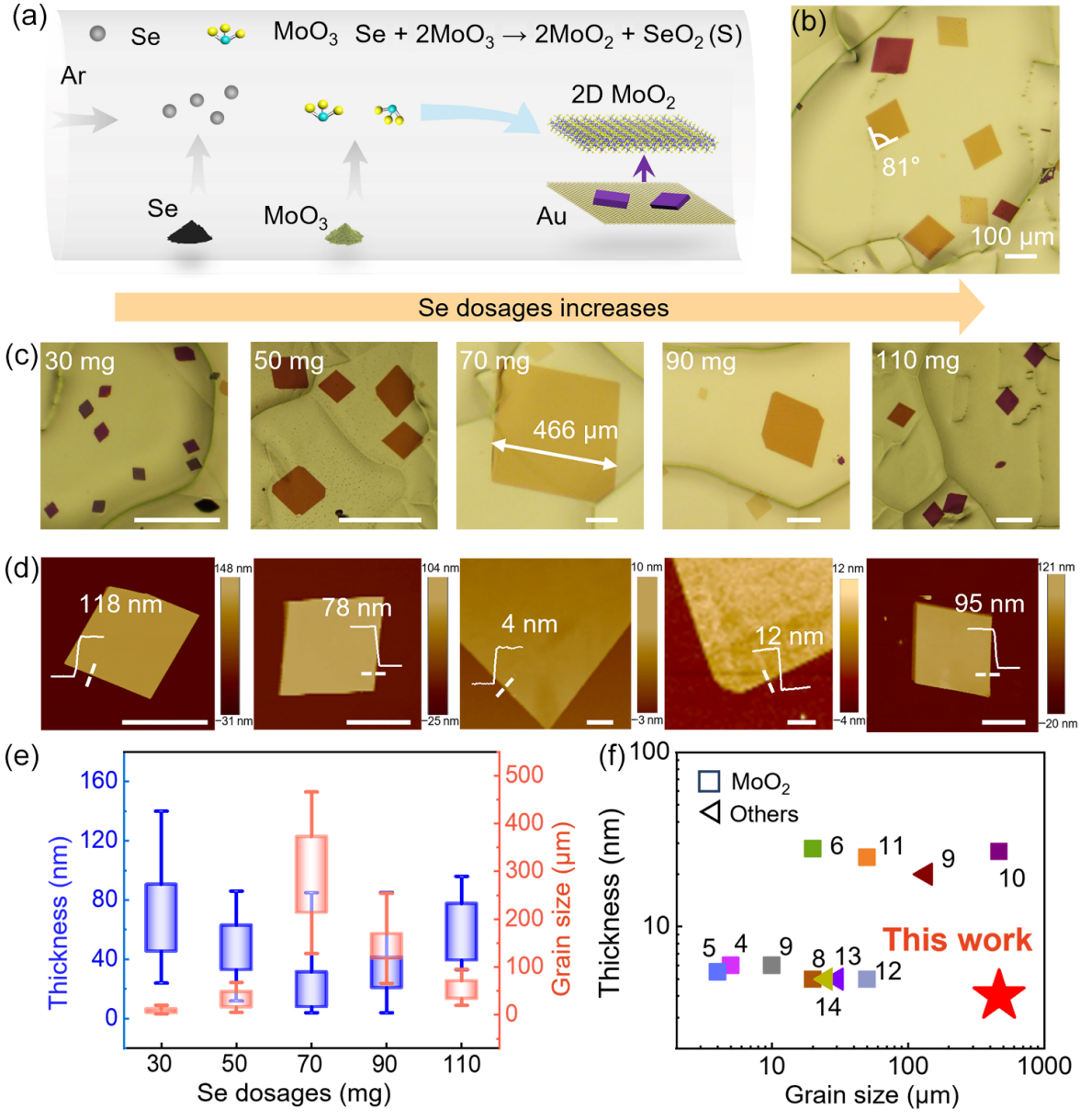

Figure 1 The synthesis of large-scale 2D MoO_2 flakes with controllable thicknesses. (a) The schematic diagram for CVD growth of 2D MoO_2. (b) Typical morphology of 2D MoO_2 flakes homogeneously distributed on Au surface. (c) Optical images of 2D MoO_2 flakes obtained with different Se dosages from 30 to 110 mg. The scale bar is 100 μm. (d) Corresponding AFM images measured from the representative MoO_2 flakes grown with different Se dosages. The scale bar is 10 μm. The AFM was implemented after the samples were transferred onto SiO_2/Si substrates by electrochemical bubbling transfer method (Fig. S1 in the ESM). (e) The statistical results of grain sizes and thicknesses, according to the randomly selected 20 samples in each optical image in Fig. S3 in the ESM. (f) The comparison of grain sizes and thicknesses of 2D metal oxides corresponding to the references in Table S1 in the ESM and this work.

respectively. The characteristic peaks at 567 and 740 cm^{-1} can be attributed to bond vibration modes (Mo–O_1 and Mo–O_2) of MoO_2, while the other fingerprint peaks represent the phonon vibration modes of MoO_2. The valence states of Mo were also detected by XPS in Fig. 2(b). Here, the adventitious carbon 1s peak at 284.8 eV was used as a reference [29]. There exist three pairs of spin-orbit doublets ($3d_{5/2}$ and $3d_{3/2}$) in Mo 3d characteristic peaks, which are fitted at 229.0 and 232.5, 231.5 and 234.7, 233.1 and 236 eV, respectively. The former two pairs are attributed to the binding energies of Mo^{4+}, while the last pair of doublets is derived from Mo^{6+}, which may be attributed to slight oxidation on the surface, contamination, and the adsorption of some MoO_3 powders [28, 29]. The intensity and area of Mo^{4+} peaks are much more than that of and Mo^{6+} peaks, indicating that molybdenum ion is mainly tetravalent as expected in MoO_2 stoichiometry. High-angle annular dark-field scanning transmission electron microscopy (HAADF-STEM) was also used to further confirm the microstructure of 2D MoO_2 flakes. Figures 2(c)–2(e) display the low-resolution STEM image of a rhombic MoO_2 flake and the corresponding EDS mappings of Mo and O elements. Figure 2(f) shows a representative HAADF-STEM of MoO_2, showing its perfect lattice structure and the spacing of (020) plane is 0.24 nm, which is consistent with the simulated atomic model. The Mo atoms are coordinated by six O atoms, forming two types of octahedrons. Such atomic structure possesses two kinds of Mo–Mo metallic bonds, which will lead to a large number of intrinsic free electrons. This is also the original

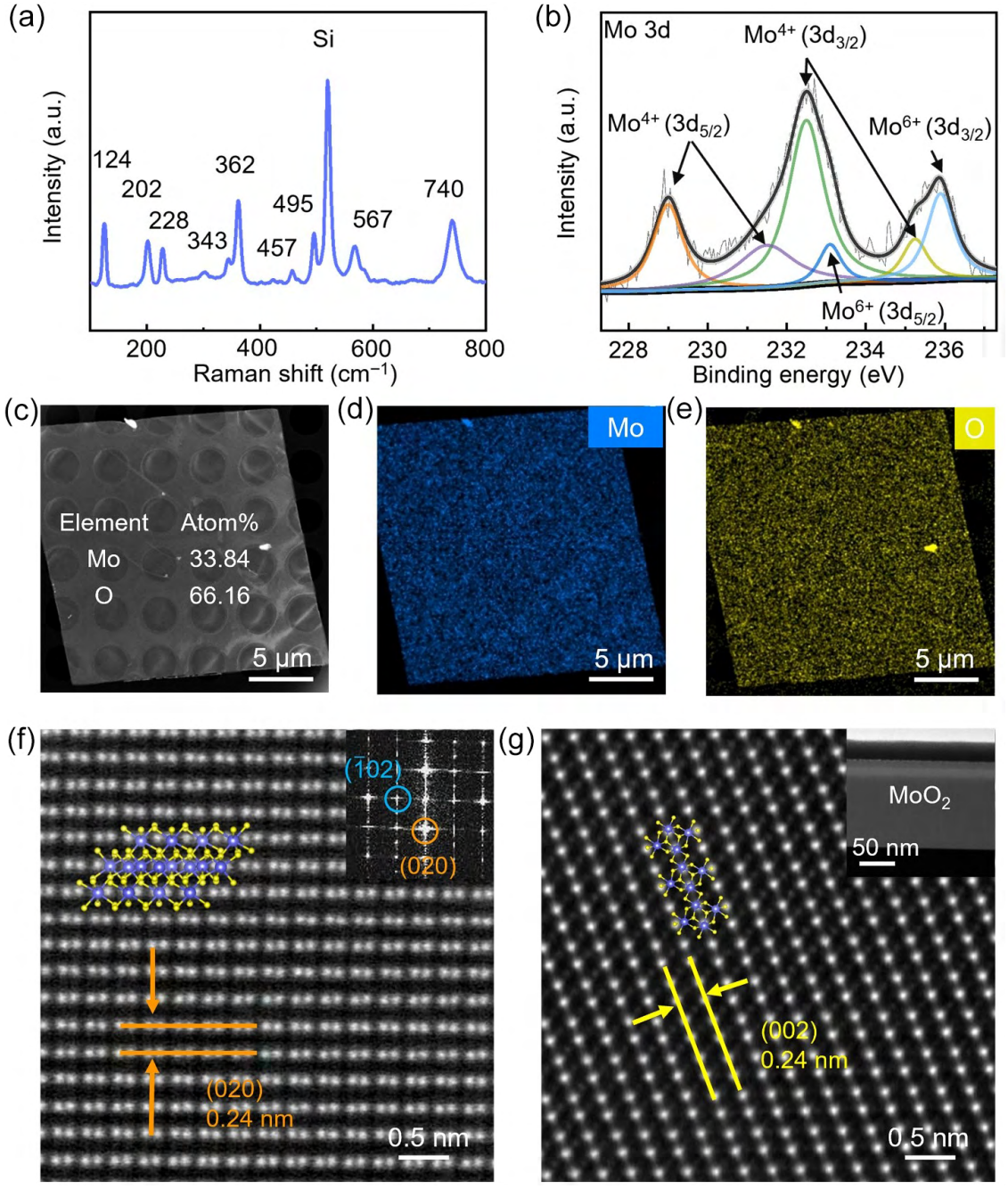

Figure 2 Structural characterization of 2D MoO_2 flakes. (a) Typical Raman spectrum of MoO_2 flakes on SiO_2/Si substrate. (b) XPS spectrum of molybdenum ion. (c) A low-resolution STEM image of a representative rhombic MoO_2 flake. Corresponding EDS mappings of (d) Mo and (e) O elements with their ratio of ~ 1:2 as shown in (c). (f) Representative HAADF-STEM image of MoO_2. The inset is the corresponding FFT pattern. (g) Cross-sectional HAADF-STEM image of MoO_2. The TEM image in the inset shows the morphology of the sample after cutting from the cross-sectional direction.

reason for the metallic feature and good SPR effect of 2D MoO_2 flakes, which will be discussed in the following text [30]. The inset is the corresponding fast Fourier transform (FFT) image, suggesting its single-crystal feature with high quality. We also observed its cross-section atomic arrangement by HAADF-STEM after cutting it through focused ion beam (FIB). The results in Fig. 2(g) further confirm the monoclinic structure of 2D MoO_2 flakes.

2.3 Noble-metal-comparable SERS performance

An ideal SERS substrate should exhibit a high EF, low LOD, high signal uniformity, excellent reproducibility, and long-term stability. To evaluate the SERS performance of 2D MoO_2 flakes, methylene blue (MeB) was employed as the main probe molecule and 532 nm laser was served as the excitation source (Fig. S4 in the ESM). As shown in Fig. 3(a), no obvious Raman signal of MeB (10^{-6} M aqueous solution) appears on bare SiO_2/Si substrates, while Raman spectra obtained from MeB on 2D MoO_2 flakes display distinct characteristic peaks at 1391 cm^{-1} (R_1) and 1625 cm^{-1} (R_2) and MoO_2 itself did not exhibit similar Raman peaks on SiO_2/Si substrates. It indicates that the Raman signal enhancement of MeB is attributed to 2D MoO_2 flakes. Interestingly, we also found that such Raman enhancement effect has a strong dependence on the thickness of 2D

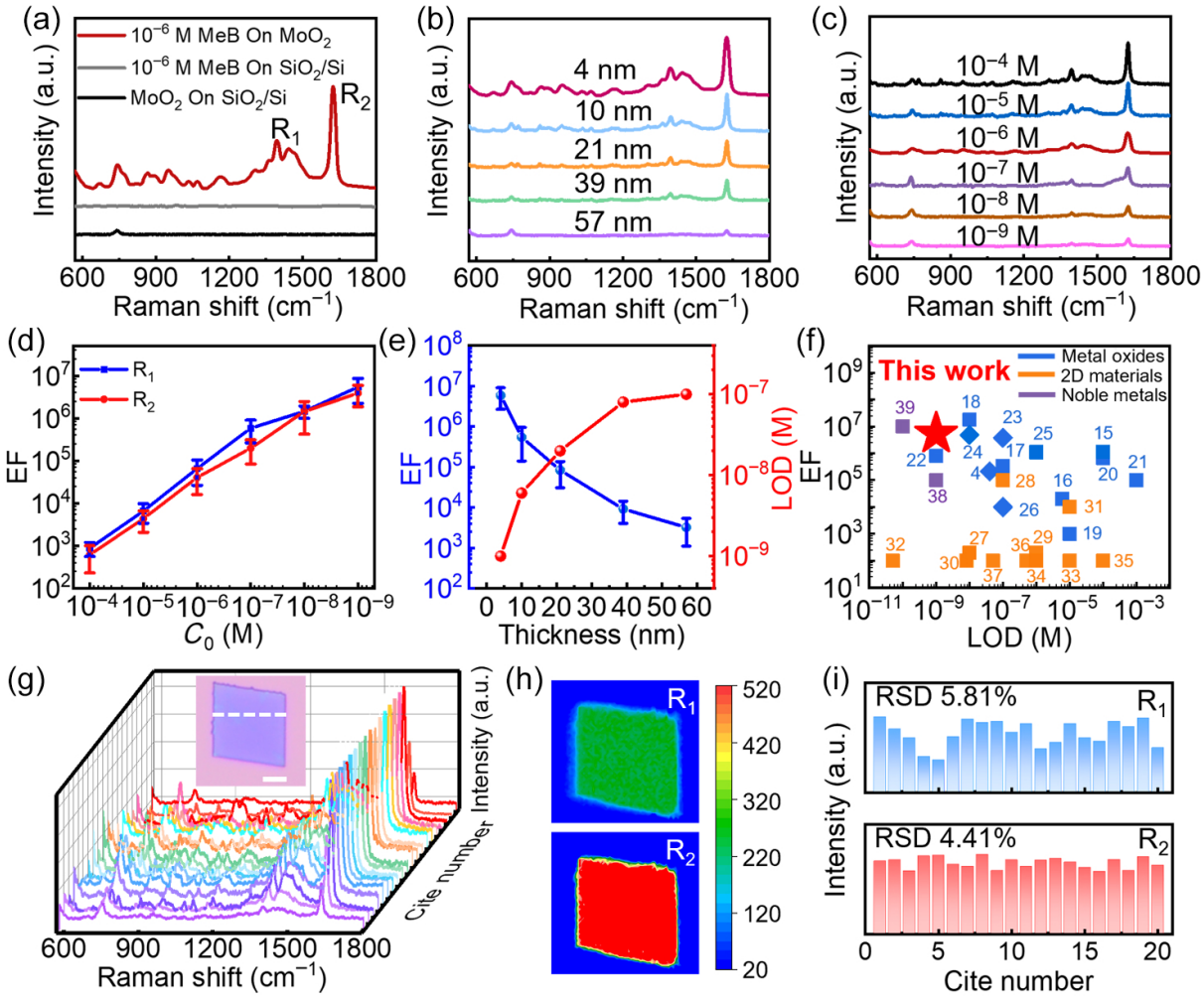

Figure 3 The noble-metal-comparable SERS performance of 2D MoO_2 flakes. (a) Raman spectra of 2D MoO_2 flake, 10^{-6} M MeB on SiO_2/Si substrate, and MeB on 2D MoO_2 flake (R_1 at 1391 cm^{-1} and R_2 at 1625 cm^{-1}), respectively. (b) Raman enhancement variation with the changing of the thickness of 2D MoO_2 flakes. (c) Raman spectra of MeB solutions with different concentrations (from 10^{-4}–10^{-9} M) on 4 nm-thick MoO_2. (d) The statistical results of corresponding enhancement factors of R_1 and R_2 peaks. (e) The enhancement effect changes of 2D MoO_2 with 5 different thicknesses on the R_2 peak of MeB. (f) The comparison of EF and LOD values obtained from 4 nm-thick MoO_2 with those from references in Table S2 in the ESM. (g) 20 Raman spectra of MeB molecules along the white dashed line in the inset which shows the optical image of 4 nm-thick MoO_2 on SiO_2/Si substrate. The scale bar is 5 μm. (h) Raman mappings of R_1 and R_2 peaks measured from 10^{-6} M MeB on the same MoO_2 flake in the inset of (g). (i) Raman intensities of R_1 and R_2 peaks collected from 20 randomly selected points on the MoO_2 flakes in (g).

MoO_2 flakes. For the same MeB aqueous solution, the enhancement of R_1 and R_2 peaks shows a stronger trend as the thickness of 2D MoO_2 flake decreases from 57 to 4 nm (Fig. 3(b) and Fig. S5 in the ESM). As shown in Fig. 3(c), we further observed the Raman signal enhancement phenomenon of MeB solutions with different concentrations (from 10^{-4} to 10^{-9} M) on 4 nm-thick MoO_2 and calculated the corresponding EFs of R_1 and R_2 peaks based on these results. To ensure the reliability of the data, we selected 20 points for each concentration of MeB solution for Raman testing (EF calculation and result statistics), as shown in Fig. 3(d). Surprisingly, EF obtained from 4 nm-thick MoO_2 can be as high as 5.4×10^6, a value higher than that of most reported metal oxides and 2D materials, even comparable to that of noble metal SERS substrates with "hot spots". Meanwhile, it can achieve trace substance detection, with its LOD as low as 10^{-9} M. Figure 3(e) shows the statistical analysis using the same calculation method to evaluate the EF and LOD of five different thicknesses of MoO_2 from Fig. 3(b), further confirming a strong thickness-dependent SERS performance. The thinner its thickness, the better its EF and LOD performance. At a thickness of 4 nm, which is the thinnest thickness reported in the current literature for large-scale 2D non-layered metal oxides materials, it exhibits the best Raman enhancement effect, as discussed in Fig. 3(d). A further comprehensive comparison of above results with the previously reported metal oxides, 2D materials and noble metal SERS substrates (Fig. 3(f) and Table S2 in the ESM) reveals that such atomic-thin metallic MoO_2 possesses high-level SERS performance and it is promising to become an ideal candidate comparable to noble metal SERS substrates.

In practical SERS applications, uniformity and reproducibility of Raman signals, as well as the stability and universality of substrate materials are also very important. Compared with noble metal SERS substrates, atomic-thin MoO_2 has a super smooth surface, which gives it a natural advantage in the uniformity of SERS signals [31, 32]. To prove this, a 4 nm-thick MoO_2 flake was used as the SERS substrate with MeB (10^{-6} M) as the probe molecule. 20 points along the white dashed line in the inset of Fig. 3(g) were chosen for SERS detection and all the Raman signals look highly similar. SERS

mappings were also performed in Fig. 3(h), both R_1 and R_2 Raman mappings show excellent uniformity within the entire MoO_2 flake. As shown in Fig. 3(i), we further calculated the relative standard deviations (RSDs) by randomly selecting 20 measurement points on the MoO_2 flake. The RSDs based on the intensities of corresponding Raman peaks R_1 and R_2 are only 5.81% and 4.41%, respectively. When the probe molecule was replaced with Rhodamine 6G (R6G), which exhibits a stronger fluorescence background than that of MeB, a similar conclusion was drawn in Fig. S6 in the ESM. All these results indicate that ultrathin 2D MoO_2 has high signal uniformity when used as a SERS substrate. In addition, it also features excellent reproducibility of SERS signals (Fig. S7(a) in the ESM) and universality for many commonly used chemicals (Fig. S8 in the ESM). 2D MoO_2 flakes exhibit strong thermal and chemical stability after high-temperature heating at 300 °C in air, as well as resistance to corrosion in strong acids or alkalis (Figs S9–S11 in the ESM).

2.4 High SERS performance realized by thickness-dependent enhancement mechanism

As shown in Figs. 4(a)–4(c), such monoclinic-phase MoO_2 presents a metallic character based on the theoretical calculations of density functional theory (DFT), which is similar to previous results [25, 28]. The calculated electron localization function (ELF) in Fig. 4(c) reveals that there is a large amount of free electron gas around Mo^{4+}, which constitutes the non-polar Mo–Mo metal bond. Due to the presence of numerous free electrons, MoO_2 has a strong SPR effect, which is also an important reason for its excellent SERS performance as discussed in Fig. 3. It is worth noting that the free electron concentration of 2D MoO_2 is related to its thickness. As shown in Figs. 4(d) and 4(e), the current–voltage curves of MoO_2 with 5 different thicknesses were conducted. It was calculated that the electrical conductivity/resistivity gradually decreased/increased with the increasing of thicknesses from 4 to 57 nm. Ultraviolet–visible (UV–vis) absorption spectra in Fig. 4(f) show that 2D MoO_2 with 5 different thicknesses all have very distinct absorption peaks, confirming the strong SPR effect as reported [25, 26, 28]. We also found that the absorption peak gradually redshifts from 550 to 570 nm with the thickness increasing. This is because the plasma energy loss of 2D MoO_2 increases with the increase of thickness, resulting in a gradual weakening of its SPR effect [28, 33]. Therefore, due to the stronger SPR effect, 4 nm-thick atomic-thin MoO_2 exhibits superior SERS performance compared to samples with other thicknesses, as discussed in Fig. 3.

On the other hand, by comparing the absorption spectra for

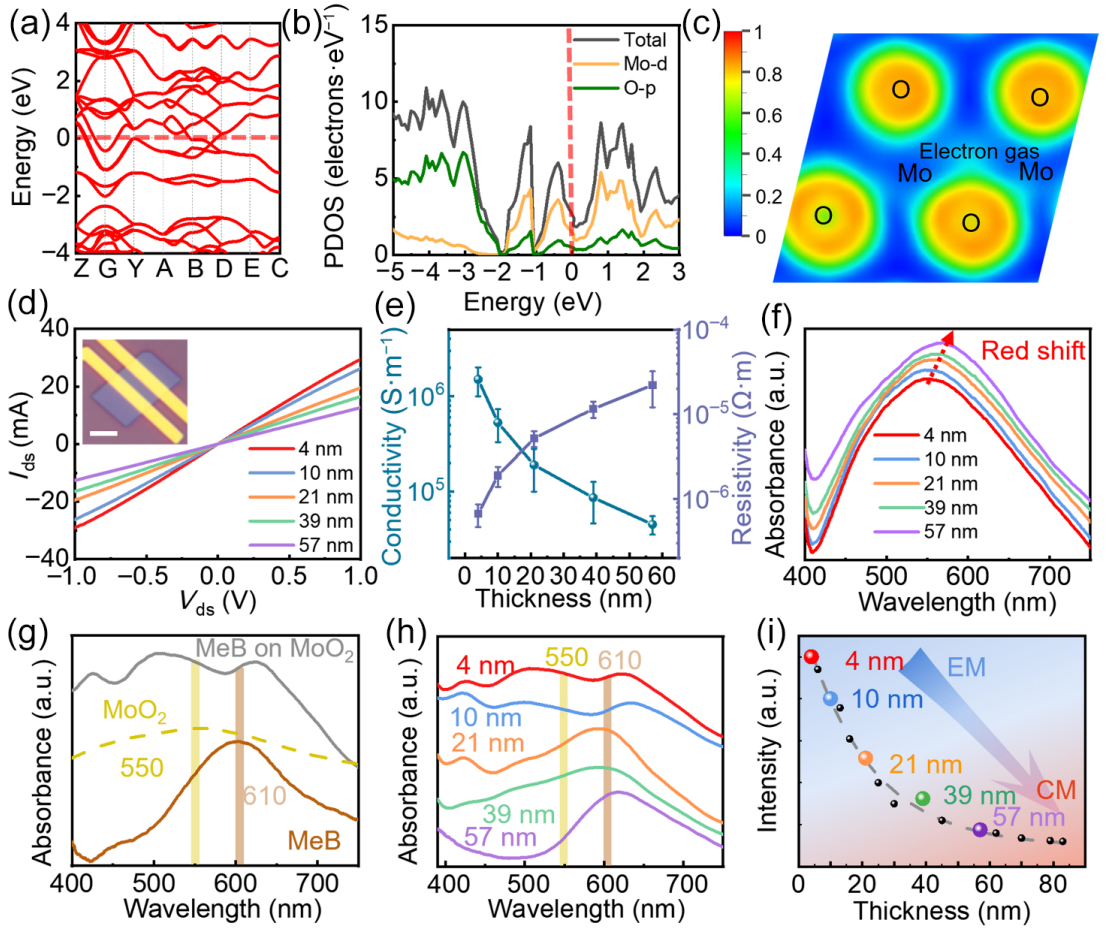

Figure 4 Thickness-dependent SPR effect and charge transfer of 2D MoO_2. (a) The band structure of MoO_2. (b) Electronic density of states for MoO_2. The highest occupied states near the Fermi level of MoO_2 are mainly composed of Mo 3d orbitals. (c) The calculated ELF of MoO_2. Charge localization gradually increases from green to orange regions. (d) A series of *I*–*V* curves obtained from MoO_2 flakes with 5 different thicknesses. The inset is a typical optical image of the device of MoO_2, the scale bar is 10 μm. (e) The corresponding conductivity and resistivity calculated from (d). (f) UV–vis absorption spectra of MoO_2 with 5 different thicknesses. (g) The comparison of absorption spectra for MeB on MoO_2 and MeB. (h) UV–vis absorption of 10^{-6} M MeB on MoO_2 substrates with 5 different thicknesses. (i) The enhanced Raman signal intensity of 10^{-6} M MeB on MoO_2 with 15 different thicknesses from 4 to 83 nm, according to the Raman spectra in Fig. 3(b) and Fig. S13 in the ESM.

MeB on MoO_2 and MeB, we found that MeB will exhibit new absorption peaks and the shift of peak position with the existence of MoO_2 as substrates (Fig. 4(g)). This can be attributed to the charge transfer process caused by the interfacial interaction between MeB molecules and MoO_2 [25, 34]. The charge difference between them was also calculated by DFT to further confirm this point of view [35]. There exists a strong chemisorption between MeB molecules and MoO_2, with an adsorption energy of about −3.49 eV (Fig. S12 in the ESM). Meanwhile, an evident charge transfer process occurs at the interface that electrons are primarily transferred from Mo atoms to the regions around N atoms of MeB molecules, indicating the strong electronic coupling and significant interfacial interaction between MeB and MoO_2.

More importantly, such charge transfer process was also related to the thickness of 2D MoO_2, as observed in Fig. 4(h). With the thickness increasing, the charge transfer phenomenon becomes more obvious, which exactly shows the opposite trend of the thickness-related SPR effect as discussed in Figs. 4(d)–4(f). It is well known that SERS substrates with strong SPR effect usually exhibit a strong EM enhancement, while the charge transfer process usually dominates the relatively weak CM enhancement [8, 36–38]. Both the SPR effect and charge transfer process of 2D MoO_2 depend on its thickness and show opposite trends, resulting in its enhancement mechanism also having obvious thickness dependence, as shown in Fig. 4(i). This means that for 2D MoO_2 with different thicknesses, both EM and CM enhancement exist simultaneously, but which one plays a dominant role varies continuously with its thickness. With increasing the thickness of 2D MoO_2, its strong SPR effect weakens while the relatively weak charge transfer process intensifies. Therefore, thinner samples show strong EM enhancement, while relatively thicker samples show relatively weak CM enhancement. Accordingly, 4 nm-thick MoO_2 exhibits superior SERS performance compared to samples with other thicknesses. Such thickness-dependent enhancement mechanism was firstly comprehensively reported for metal oxide-based SERS substrates.

2.5 Applications in image security and information encryption

Atomic-thin MoO_2 not only has SERS performance comparable to that of noble metals with "hot spots", but also features precise signal recognition and strong anti-interference ability. It is expected to be applied in high-tech fields such as layer information encryption and image anti-counterfeiting. For instance, after the same MoO_2 sample was successively immersed in three different aqueous solutions of R6G, MV, and MeB (see Experimental), the Raman signal was tested. As shown in Fig. 5(a), the Raman characteristic peaks of each organic compound could be fully displayed without interfering with each other. Then, we formed a 5 × 5 rectangular array with 25 ultra-thin MoO_2 flakes (each square in the matrix is 25 μm × 25 μm). The array was patterned by deposited R6G, MV, and MeB aqueous solutions, respectively forming the corresponding N, E, and U graphs as shown in Fig. 5(b). When the Raman characteristic peak of a specific organic compound is selected as the test object, the matrix will display the corresponding character graphic, thereby achieving a simple information encryption function. For specific examples, when the Raman peaks marked by the red, blue, and yellow dotted areas in Fig. 5(a) are tested respectively, the matrix area will correspondingly show the N, E, and U graphs pre-deposited by R6G, MV, and MeB. When cracking encrypted information, we can obtain the marked graphics one by one by providing the characteristic peaks, sequences and occurrence frequencies of individual organic substances, and then display the encrypted information. As shown in Fig. 5(c), when the decrypted numbers are 612, 912, 770, and 985, we can obtain the image information of NENU.

In addition, after calibrating several different components of the image with different organic substances and selecting specific Raman peaks for detection, it is possible to selectively display part or the entire image information to achieve the purpose of image anti-counterfeiting. As shown in Fig. S14(a) in the ESM, we constructed an array of panda images using several ultrathin MoO_2 flakes, and labeled the panda eyes, panda contours and bamboo parts in the images with R6G, MV and MeB, respectively (Fig. 5(d)). When detecting the Raman signal mapping of the entire image array, choosing an appropriate measurement range can display partial images of a single organic label (Figs. S14(b)–S14(d) in the ESM), or partial combined images of more than two organic labels. For example, when the test range is 1150–1200 cm^{-1} (the area marked by the purple dotted line in Fig. 5(a)) and 1600–1669 cm^{-1}, the patterns shown in Figs. 5(e) and 5(f) will be displayed respectively.

3 Conclusion

In summary, large-scale (~ 466 μm) atomic-thin (~ 4 nm) metallic MoO_2 was firstly synthesized by Se-assisted CVD. It shows high SERS sensitivity with detected concentration down to 10^{-9} M and a maximum EF up to 10^7, which is at a high level among most metal oxide-based SERS substrates, and even comparable to the values of noble metal substrates with "hot spots". Both the SPR effect and charge transfer process of 2D MoO_2 depend on its thickness and show opposite trends, resulting in its enhancement mechanism also having obvious thickness dependence. It means that both EM and CM enhancement exist simultaneously, but which one plays a dominant role varies continuously with thicknesses. Therefore, 4 nm-thick MoO_2 exhibits superior SERS performance compared to samples with other thicknesses due to the relatively stronger EM enhancement induced by SPR effect. In addition, it also features excellent reproducibility of SERS signals, good stability, as well as universality for a variety of detected substances. Large-scale 2D metallic MoO_2 is not only an ideal substrate for SERS, but also potential in image security and information encryption. This work offers important insights for the synthesis of non-layered metal oxides and other 2D materials, which can help develop the SERS performance and applications with 2D metal oxide-based substrate materials.

4 Experimental

4.1 Growth 2D MoO_2 on Au by CVD

2D MoO_2 flakes were synthesized by CVD in a tube furnace. Au foil (99.99 wt.%, 100 μm-thick, 1 cm × 1 cm, Beijing Kairi Material Technology Co., LTD.) was ultrasonically cleaned with acetone, isopropyl alcohol and ethanol for 20 min, and then annealed at 1050 °C in air for more than 10 h. Firstly, the annealed Au foil was placed in the center of the quartz tube, and 100 mg MoO_3 powder (99.999 wt.%, Adamas) was placed 3 cm upstream of the Au foil. 70 mg Se powder (99.99 wt.%, Aladdin) was heated separately and placed upstream of outside the high temperature zone. The distance between selenium powder and Au foil was about 18.5 cm. The

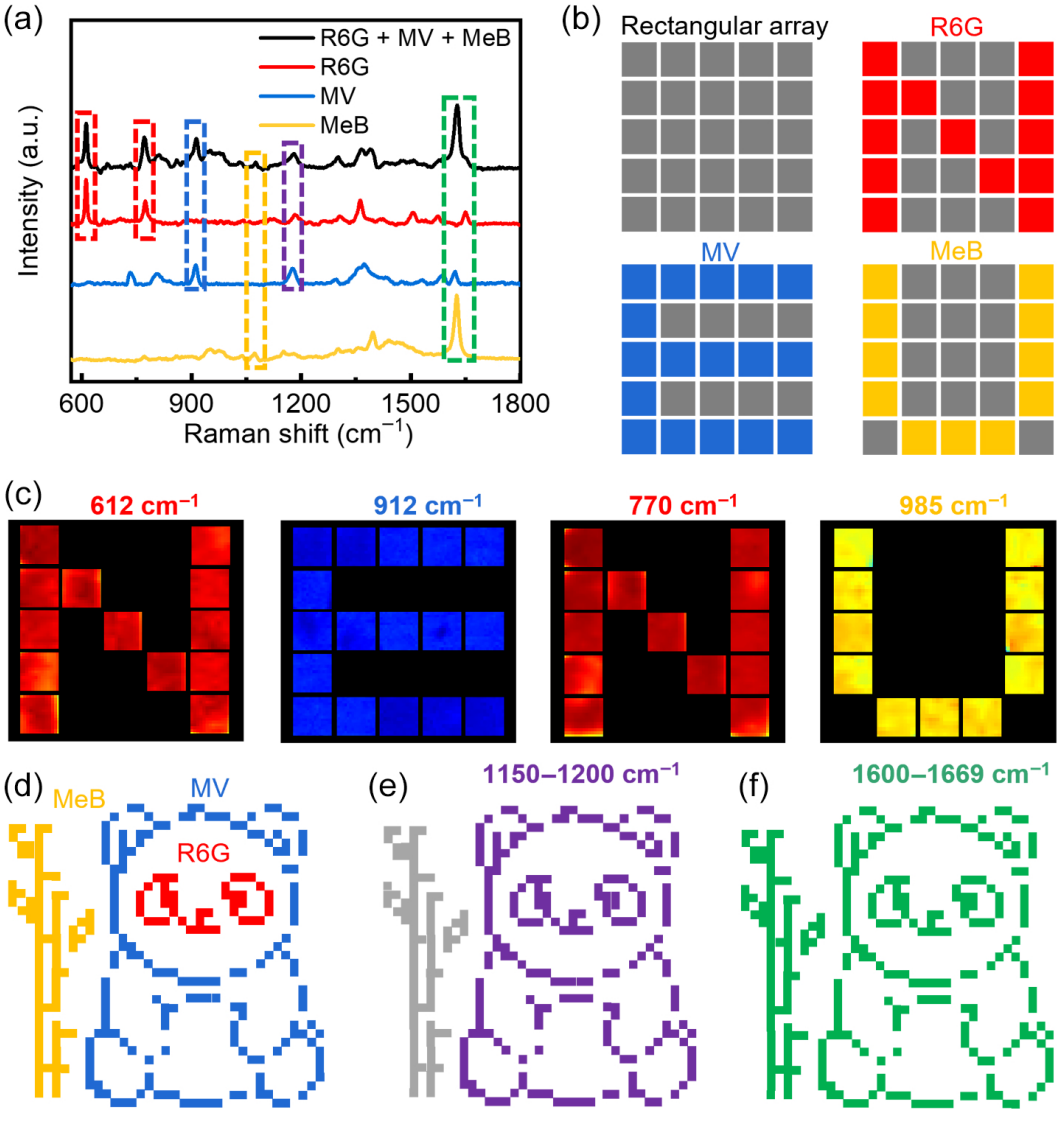

Figure 5 2D MoO_2 substrates for graphic information encryption and image security. (a) Raman peaks marked by the red, blue, and yellow dotted lines show the characteristic peaks of R6G, MV, and MeB on MoO_2 flakes, respectively. (b) A 5 × 5 rectangular array based on 25 ultra-thin MoO_2 flakes. The thickness range of the MoO_2 flakes is 4–10 nm and the size of each square in the array is 25 μm. (c) The obtained image information of NENU by selecting Raman peaks at 612, 912, 770, and 985 cm^{-1}, respectively. (d)–(f) An array of panda images using several ultrathin MoO_2 flakes. Panda eyes, panda contours, and bamboo parts were labeled with R6G, MV, and MeB, respectively. Partial or complete patterns can be displayed by selecting an appropriate measurement range.

furnace was heated from room temperature to 750 °C in 30 min and 900 °C in 10 min. When the furnace was heated to 900 °C, MoO_2 was grown on substrate after growth process lasted for 6 min. 100 standard cubic centimeter per minute (sccm) argon gas was introduced into the whole process. The sample was cooled rapidly to room temperature.

4.2 Characterization

The morphology of MoO_2 was characterized by optical microscopy (Olympus BX51 microscope). An atomic force microscope (AFM, Bruker Dimension Icon) system was used to determine the thickness of MoO_2. XPS (ESCALAB 250) was used to characterize the chemical composition of MoO_2. The atomic structure of MoO_2 was carried out by TEM on an FEI Titan Themis Cube with an X-FEG electron gun and a DCOR aberration corrector operating at 100 kV. UV–vis absorption spectroscopy was used by a commercial integrated platform including xenon lamp (300–1100 nm).

4.3 Devices fabrication and electrical property measurements

MoO_2 was transferred onto Si substrates with a 280 nm-thick SiO_2 layer. Then, the 10 nm Ti/50 nm Au layer electrodes were deposited by electron beam evaporation. An agilent semiconductor parameter analyzer (4155C Semiconductor Parameter Analyser) was used to measure the electrical properties at room temperature.

4.4 Raman test

Raman spectra were obtained with a Raman spectrometer (JY HR-800 LabRAM) by using a 532 nm semiconductor laser (output power: 50 mW, spot size: 1 μm) as the excitation source. R6G, MeB, MB, RhB, and MV dissolved in deionized water were employed to be the probe molecules. The stock solutions were prepared at a concentration of 10^{-4} M and then diluted to 10^{-5}, 10^{-6}, 10^{-7}, 10^{-8}, and 10^{-9} M. In the section of LOD, signal uniformity and reproducibility

of SERS, 2D MoO_2 substrates were soaked in a series of concentrations of aqueous solution for 30 min, and dried in a clean N_2 atmosphere. In the section of EF calculation and graphic information encryption and image security, several microliters of aqueous solution of organic molecules were dripped onto the substrate surface and dried naturally in the air before conducting the Raman test. Then, the same type of confocal Raman spectrometer was used to collect the Raman spectrum, using a 532 nm laser with 5 mW power, 50 × objective lens, and a single acquisition time of 10 s. The acquisition time of Raman mapping was 1 s. By fitting a polynomial, the background of all Raman spectra was extracted and removed.

4.5 DFT calculations

The DFT calculations of monoclinic MoO_2 were performed using the generalized gradient approximation (GGA)/Perdew–Burke–Ernzerhof (PBE) as the exchange-correlation functional in the Vienna *ab initio* simulation package (VASP) and DFT-D3 for van der Waals (vdW) correction. Starting from the experimental crystal structure of monoclinic MoO_2 (space group: P_{21}/c), the cell parameters and atomic positions were further relaxed until the total Hellmann–Feynman forces on each atom were < 0.01 eV·Å^{-1}. The uniform Brillouin zone grids of 5 × 6 × 5 K point for geometry optimization were used and the plane-wave basis set cutoff of the wavefunctions was set at 500 eV.

The charge density difference between MeB and MoO_2 was calculated using the VASP. The electron-ion interactions were described by projector augmented wave (PAW) method. The exchange-correlation interactions were conducted with the PBE functional within the GGA. DFT-D3 correction was employed for long-range van der Waals interactions. To account for the solvation effect in aqueous environments, the implicit solvation model implemented in VASPsol was used. The plane-wave cutoff energy was 520 eV for both structural optimizations and self-consistent calculations. The convergence criteria for electronic and ionic relaxations were 1×10^{-5} eV per atom and 0.05 eV·Å^{-1}, respectively.

Electronic Supplementary Material: Supplementary material (details of CVD preparation, Raman detection, EF calculation, SERS performance, and DFT analysis) is available in the online version of this article at https://doi.org/10.26599/NR.2026.94908825.

Data availability

All data needed to support the conclusions in the paper are presented in the manuscript and the Electronic Supplementary Material. Additional data related to this paper may be requested from the corresponding author upon request.

Acknowledgements

This work was supported by the National Key Research and Development Program of China (No. 2023YFB3610200), the Program of Natural Science Foundation of China (Nos. 52002056, 12274065, 62275045, and 62574038), the Fundamental Research Funds for the Central Universities (No. 2412025PD013), the Science and Technology Development Plan Project of Jilin Province (No. 20240601049RC), the Foundation of Jilin Educational Committee of China (No. JJKH20221151KJ), and the Natural Science Foundation of Jilin Province (No. 20240101318JC). The authors sincerely acknowledge Dr. H. Zhu and Dr. G. Wang for providing technology supporting on characterization of the samples.

Declaration of competing interest

All the contributing authors declare no conflict of interests in this work.

Author contribution statement

Y. Z. B.: Data curation, project administration, validation, writing manuscript, experimental design. J. M. C., M. F. D. and D. M. C.: Data curation. J. Z.: validation. X. X.: Project administration, funding acquisition. W. X., W. Z. L., P. L., J. G. M., H. Y. X., and Y. C. L.: Project administration, funding acquisition. All the authors have approved the final manuscript.

Use of AI statement

None.

References

[1] Cialla, D.; März, A.; Böhme, R.; Theil, F.; Weber, K.; Schmitt, M.; Popp, J. Surface-enhanced Raman spectroscopy (SERS): Progress and trends. *Anal. Bioanal. Chem.* **2012**, *403*, 27–54.

[2] Pilot, R.; Signorini, R.; Durante, C.; Orian, L.; Bhamidipati, M.; Fabris, L. A review on surface-enhanced Raman scattering. *Biosensors* **2019**, *9*, 57.

[3] Sharma, B.; Frontiera, R. R.; Henry, A. I.; Ringe, E.; Van Duyne, R. P. SERS: Materials, applications, and the future. *Mater. Today* **2012**, *15*, 16–25.

[4] Cao, Y. W. C.; Jin, R. C.; Mirkin, C. A. Nanoparticles with Raman spectroscopic fingerprints for DNA and RNA detection. *Science* **2002**, *297*, 1536–1540.

[5] Mulvihill, M.; Tao, A.; Benjauthrit, K.; Arnold, J.; Yang, P. D. Surface-enhanced Raman spectroscopy for trace arsenic detection in contaminated water. *Angew. Chem., Int. Ed.* **2008**, *47*, 6456–6460.

[6] Schlücker, S. Surface-enhanced Raman spectroscopy: Concepts and chemical applications. *Angew. Chem., Int. Ed.* **2014**, *53*, 4756–4795.

[7] Laing, S.; Jamieson, L. E.; Faulds, K.; Graham, D. Surface-enhanced Raman spectroscopy for *in vivo* biosensing. *Nat. Rev. Chem.* **2017**, *1*, 0060.

[8] Cardinal, M. F.; Ende, E. V.; Hackler, R. A.; McAnally, M. O.; Stair, P. C.; Schatz, G. C.; Van Duyne, R. P. Expanding applications of SERS through versatile nanomaterials engineering. *Chem. Soc. Rev.* **2017**, *46*, 3886–3903.

[9] Ding, S. Y.; You, E. M.; Tian, Z. Q.; Moskovits, M. Electromagnetic theories of surface-enhanced Raman spectroscopy. *Chem. Soc. Rev.* **2017**, *46*, 4042–4076.

[10] Kanipe, K. N.; Chidester, P. P. F.; Stucky, G. D.; Moskovits, M. Large format surface-enhanced Raman spectroscopy substrate optimized for enhancement and uniformity. *ACS Nano* **2016**, *10*, 7566–7571.

[11] Zhu, C. H.; Meng, G. W.; Zheng, P.; Huang, Q.; Li, Z. B.; Hu, X. Y.; Wang, X. J.; Huang, Z. L.; Li, F. D.; Wu, N. Q. A hierarchically ordered array of silver-nanorod bundles for surface-enhanced Raman scattering detection of phenolic pollutants. *Adv. Mater.* **2016**, *28*, 4871–4876.

[12] Zheng, Z. H.; Cong, S.; Gong, W. B.; Xuan, J. N.; Li, G. H.; Lu, W. B.; Geng, F. X.; Zhao, Z. G. Semiconductor SERS enhancement enabled by oxygen incorporation. *Nat. Commun.* **2017**, *8*, 1993.

[13] Wang, Y. F.; Ruan, W. D.; Zhang, J. H.; Yang, B.; Xu, W. Q.; Zhao, B.; Lombardi, J. R. Direct observation of surface-enhanced Raman

scattering in ZnO nanocrystals. *J. Raman Spectrosc.* **2009**, *40*, 1072–1077.

[14] Gordon, T. R.; Cargnello, M.; Paik, T.; Mangolini, F.; Weber, R. T.; Fornasiero, P.; Murray, C. B. Nonaqueous synthesis of TiO_2 nanocrystals using TiF_4 to engineer morphology, oxygen vacancy concentration, and photocatalytic activity. *J. Am. Chem. Soc.* **2012**, *134*, 6751–6761.

[15] Jiang, L.; You, T. T.; Yin, P. G.; Shang, Y.; Zhang, D. F.; Guo, L.; Yang, S. H. Surface-enhanced Raman scattering spectra of adsorbates on Cu_2O nanospheres: Charge-transfer and electromagnetic enhancement. *Nanoscale* **2013**, *5*, 2784–2789.

[16] Xi, G. C.; Ouyang, S. X.; Li, P.; Ye, J. H.; Ma, Q.; Su, N.; Bai, H.; Wang, C. Ultrathin $W_{18}O_{49}$ nanowires with diameters below 1 nm: Synthesis, near-infrared absorption, photoluminescence, and photochemical reduction of carbon dioxide. *Angew. Chem., Int. Ed.* **2012**, *51*, 2395–2399.

[17] Lin, J.; Shang, Y.; Li, X. X.; Yu, J.; Wang, X. T.; Guo, L. Ultrasensitive SERS detection by defect engineering on single Cu_2O superstructure particle. *Adv. Mater.* **2017**, *29*, 1604797.

[18] Qi, D. Y.; Lu, L. J.; Wang, L. Z.; Zhang, J. L. Improved SERS sensitivity on plasmon-free TiO_2 photonic microarray by enhancing light-matter coupling. *J. Am. Chem. Soc.* **2014**, *136*, 9886–9889.

[19] Xu, W. G.; Mao, N. N.; Zhang, J. Graphene: A platform for surface-enhanced Raman spectroscopy. *Small* **2013**, *9*, 1206–1224.

[20] Ling, X.; Xie, L. M.; Fang, Y.; Xu, H.; Zhang, H. L.; Kong, J.; Dresselhaus, M. S.; Zhang, J.; Liu, Z. F. Can graphene be used as a substrate for Raman enhancement. *Nano Lett.* **2010**, *10*, 553–561.

[21] Xie, L. M.; Ling, X.; Fang, Y.; Zhang, J.; Liu, Z. F. Graphene as a substrate to suppress fluorescence in resonance Raman spectroscopy. *J. Am. Chem. Soc.* **2009**, *131*, 9890–9891.

[22] Xu, H.; Xie, L. M.; Zhang, H. L.; Zhang, J. Effect of graphene fermi level on the Raman scattering intensity of molecules on graphene. *ACS Nano* **2011**, *5*, 5338–5344.

[23] Sun, L. F.; Hu, H. L.; Zhan, D.; Yan, J. X.; Liu, L.; Teguh, J. S.; Yeow, E. K. L.; Lee, P. S.; Shen, Z. X. Plasma modified MoS_2 nanoflakes for surface enhanced Raman scattering. *Small* **2014**, *10*, 1090–1095.

[24] Zaleski, S.; Wilson, A. J.; Mattei, M.; Chen, X.; Goubert, G.; Cardinal, M. F.; Willets, K. A.; Van Duyne, R. P. Investigating nanoscale electrochemistry with surface-and tip-enhanced Raman spectroscopy. *Acc. Chem. Res.* **2016**, *49*, 2023–2030.

[25] Zhang, Q. Q.; Li, X. S.; Ma, Q.; Zhang, Q.; Bai, H.; Yi, W. C.; Liu, J. Y.; Han, J.; Xi, G. C. A metallic molybdenum dioxide with high stability for surface enhanced Raman spectroscopy. *Nat. Commun.* **2017**, *8*, 14903.

[26] Zhang, Q. Q.; Li, X. S.; Yi, W. C.; Li, W. T.; Bai, H.; Liu, J. Y.; Xi, G. C. Plasmonic MoO_2 nanospheres as a highly sensitive and stable non-noble metal substrate for multicomponent surface-enhanced Raman analysis. *Anal. Chem.* **2017**, *89*, 11765–11771.

[27] Lin, X. C.; Yan, P. F.; Xu, F. F.; Wu, W. Z.; Hu, T. Z.; Wei, C.; Xu, Q. Solid-phase synthesis of atomically thin two-dimensional non-layered MoO_2 nanosheets for surface enhanced Raman spectroscopy. *J. Mater. Chem. C* **2019**, *7*, 7196–7200.

[28] Wu, H. R.; Zhou, X. C.; Li, J. D.; Li, X. M.; Li, B. W.; Fei, W. W.; Zhou, J. X.; Yin, J.; Guo, W. L. Ultrathin molybdenum dioxide nanosheets as uniform and reusable surface-enhanced Raman spectroscopy substrates with high sensitivity. *Small* **2018**, *14*, 1802276.

[29] Apte, A.; Mozaffari, K.; Samghabadi, F. S.; Hachtel, J. A.; Chang, L.; Susarla, S.; Idrobo, J. C.; Moore, D. C.; Glavin, N. R.; Litvinov, D. et al. 2D electrets of ultrathin MoO_2 with apparent piezoelectricity. *Adv. Mater.* **2020**, *32*, 2000006.

[30] Zhu, Y. P.; El-Demellawi, J. K.; Yin, J.; Lopatin, S.; Lei, Y. J.; Liu, Z. X.; Miao, X. H.; Mohammed, O. F.; Alshareef, H. N. Unprecedented surface plasmon modes in monoclinic MoO_2 nanostructures. *Adv. Mater.* **2020**, *32*, 1908392.

[31] Lin, X. M.; Cui, Y.; Xu, Y. H.; Ren, B.; Tian, Z. Q. Surface-enhanced Raman spectroscopy: Substrate-related issues. *Anal. Bioanal. Chem.* **2009**, *394*, 1729–1745.

[32] Xu, W. G.; Ling, X.; Xiao, J. Q.; Dresselhaus, M. S.; Kong, J.; Xu, H. X.; Liu, Z. F.; Zhang, J. Surface enhanced Raman spectroscopy on a flat graphene surface. *Proc. Natl. Acad. Sci. USA* **2012**, *109*, 9281–9286.

[33] Raether, H. Surface plasma oscillations as a tool for surface examinations. *Surf. Sci.* **1967**, *8*, 233–246.

[34] Tian, Z.; Bai, H.; Chen, C.; Ye, Y. T.; Kong, Q. H.; Li, Y. H.; Fan, W. H.; Yi, W. C.; Xi, G. C. Quasi-metal for highly sensitive and stable surface-enhanced Raman scattering. *iScience* **2019**, *19*, 836–849.

[35] Yang, L. C. Q.; Zong, Y. J.; Yin, M.; Yi, W. C.; Li, J. F.; Lin, J.; Kong, Q. H.; Xi, G. C. Single-crystal-ordered-mesoporous metal nitrides without intrinsic Raman signals for highly sensitive SERS detection. *Chem. Sci.* **2026**, *17*, 6632–6643.

[36] Zrimsek, A. B.; Chiang, N.; Mattei, M.; Zaleski, S.; McAnally, M. O.; Chapman, C. T.; Henry, A. I.; Schatz, G. C.; Van Duyne, R. P. Single-molecule chemistry with surface-and tip-enhanced Raman spectroscopy. *Chem. Rev.* **2017**, *117*, 7583–7613.

[37] Otto, A.; Mrozek, I.; Grabhorn, H.; Akemann, W. Surface-enhanced Raman scattering. *J. Phys. Condens. Matter* **1992**, *4*, 1143–1212.

[38] Han, X. X.; Ji, W.; Zhao, B.; Ozaki, Y. Semiconductor-enhanced Raman scattering: Active nanomaterials and applications. *Nanoscale* **2017**, *9*, 4847–4861.